J Nanopart Res (2014) 16:2729
DOI 10.1007/s11051-014-2729-z

BRIEF COMMUNICATION

Long-term stability of surfactant-free gold nanostars

Marienette Morales Vega · Alois Bonifacio · Vanni Lughi · Stefano Marsi · Sergio Carrato · Valter Sergo

Received: 6 July 2014 / Accepted: 1 November 2014 / Published online: 9 November 2014

Abstract This work investigates the long-term stability of suspensions of surfactant-free gold nanostars with mean diameter of 78 ± 13 nm (measured from tip to tip across the nanostar).We monitored the optical and morphological properties of the nanostars over the course of several days after synthesis by observing the changes in the UV–visible absorption spectra and mean radius of curvature of the nanostar tips. An aging process can be observed, evident in the blunting of the nanostar tips, leading to a blue shift in the absorption maximum. Stability is greatly improved by depositing on the nanostars a monolayer of mercaptopropionic acid (MPA), possibly because of the formation of the gold–sulfur (Au–S) bond that limits the mobility of the Au atoms. Capping the nanostars with MPA is an easy additional step for extending the stability of the nanostars in suspension without significantly affecting the original plasmonic resonance band.

Keywords Gold nanostars · Nanoparticles · Surfactant-free · Aging · Stability · Mercaptopropionic acid

M. M. Vega (✉) · A. Bonifacio · V. Lughi · S. Marsi · S. Carrato · V. Sergo
Department of Engineering and Architecture, University of Trieste, Via Valerio 6/a, 34127 Trieste, Italy
e-mail: marienettemorales.vega@phd.units.it

Introduction

Nanoparticles of various shapes, sizes, and compositions have been studied for a wide variety of applications, a non-comprehensive listing of which includes drug delivery (Yuan et al. 2012b; Nam et al. 2013), cancer diagnosis (Tamburro et al. 2011) and therapy (Cheng et al. 2011), contrast enhancers for imaging (Allijn et al. 2013), as well as surface-enhanced Raman spectroscopy (SERS) (Yuan et al. 2012a; Liu and Wu 2013; Jarvis and Goodacre 2004; Kastanos et al. 2009). Nanoparticles are relatively straightforward and inexpensive to synthesize through wet chemical preparation techniques. Well-known routes are available for almost any desired morphology. Of particular interest for SERS are branched gold nanoparticles, or nanostars, because of their peculiar plasmonic properties (Hao et al. 2007; Casu et al. 2012; Guerrero-Martinez et al. 2011; Rodriguez-Oliveros and Sanchez-Gil 2012; Kooij et al. 2012).

At present, many sophisticated synthetic routes ranging from seed-mediated (Kooij et al. 2012; Wu et al. 2009; Wheeler et al. 2012; Casu et al. 2012; Yuan et al. 2012c) to one-pot methods (Hrelescu et al. 2009; Trigari et al. 2011) are widely available for nanostars. The most common seed-mediated synthesis requires the use of cetyltrimethylammonium bromide (CTAB) (Rodriguez-Lorenzo et al. 2011; Esenturk and Walker 2009; Ahmed et al. 2010), polyvinylpyrrolidone (PVP), *N,N*-dimethylformamide (DMF) solution (Kumar et al. 2008; Khoury and Vo-Dinh 2008), and

hydrazine (Jeong et al. 2009). Unfortunately, these surfactants are generally difficult to replace and challenging to functionalize for further applications (Trigari et al. 2011). Notable exceptions are the works of Casu et al. (2012) and Pallavicini et al. (2013), who have addressed this problem using zwitterionic lauryl sulfobetaine (LSB) surfactant, which gets easily removed compared to CTAB.

The straightforward synthesis of stable gold nanostars with no impeding outer layer is attractive from the viewpoint of applications. Yuan et al. (2012c) recently reported a protocol for producing surfactant-free nanostars with very little amount of citrate, a well-known biocompatible electrostatic stabilizer for gold nanoparticles. This protocol proves to be cost- and time-effective, in spite of being a seed-mediated route. However, in using this protocol, we have observed the occurrence of rapid aging (within 5 to 10 h) in all our suspensions of surfactant-free gold nanostars; hereafter, by aging we mean a morphological change of the nanoparticles that is reflected in the UV–visible absorbance spectrum. To our best knowledge, long-term stability and aging studies on surfactant-free nanostars have not been previously reported. A few papers on the stability of surfactant-stabilized nanoparticles exist. The stability studies performed by Trigari et al. (2011) were done solely on nanostars fabricated with CTAB capping and they found that even in the presence of surfactant, the nanostars can degrade after aging in suspension for some hours. Nanostars generally need to be coated to maintain stability. The use of thiolated compounds to maintain stability of nanostars is now becoming a standard. Examples of thiol-coated gold nanostars that gained excellent stability after surface coating with polyethyleneglycol-thiol (PEG-SH) were demonstrated in the works of Sironi et al. (2012) and Cavallaro et al. (2013). Another stability study was done by Gao et al. (2012), who used tandem coating of PEG-SH and MPA on spherical gold nanoparticles. Unlike these previous works, we focus on surfactant-free nanostars. We study the morphology and optical properties of surfactant-free nanostars upon aging at 4 °C, i.e., the common conditions of conservation for such kind of particles. We then propose to improve the existing protocol by forming a monolayer of MPA via Au–S bonding. One of the advantages of this approach is the solubility of MPA in water, which allows carrying out surface modification in an entirely aqueous environment.

Materials and methods

Sodium tetrachloroaurate (III) dehydrate ($AuCl_4$-$Na{\cdot}2H_2O$), sodium citrate tribasic dihydrate (Na_3C_6-$H5O_7{\cdot}2H_2O$), hydrochloric acid (HCl), silver nitrate ($AgNO_3$), L-ascorbic acid ($C6H_8O_6$), and 3-mercaptopropionic acid ($C_3H_6O_2S$) were purchased from Sigma-Aldrich and used without further purification. Milli-Q water was used for the preparation of all solutions.

According to the protocol proposed by Yuan et al. (2012c), we first synthesized spherical gold seeds. In a typical synthesis, aqueous solution of $AuCl_4$-$Na{\cdot}2H_2O$ (100 ml, 1 mM) is brought to boiling point followed by rapid addition of sodium citrate (15 ml, 1 wt%). The solution was allowed to reflux for 15 min under vigorous stirring. After cooling down, the solution is kept at 4 °C. We then produced the nanostars by preparing a growth solution consisting of $AuCl_4Na{\cdot}2H_2O$ (10 ml, 0.25 mM), HCl (10 µl, 1 M), and 100 µl of gold seeds. Under moderate stirring, ascorbic acid (50 µl, 100 mM) and $AgNO_3$ (100 µl, 1.5 mM) were simultaneously added. Instantly, a bluish-black color is achieved. We performed centrifugal washing at 3,500 rpm for 30 min. The extracted nanostars were redispersed in Milli-Q water and filtered with a 0.22-µm nitrocellulose membrane. The final product was kept at 4 °C. Surface modification of nanostars with MPA was done immediately after filtration by adding MPA (10 µl, 20 mM) to 10 ml of nanostars under vigorous stirring. The mixture was continuously stirred for 10 min at room temperature. No further centrifugal washing was done.

Absorption spectra in the wavelength range of 400–800 nm were measured using UV–vis spectrophotometer (Perkin-Elmer, Lambda 20 Bio). The morphological features of the particles were characterized by Transmission Electron Microscope (TEM, Philips EM 208). The nanostar colloids were monitored for several days after the synthesis. On the day of the measurement, suspensions were sonicated for 10 min before recording the UV–vis spectrum. An aliquot was further diluted to 10 % of the original stock concentration and 10 µl was drop cast onto a carbon TEM grid. The grid was dried at ambient temperature and TEM images were obtained on the same day of deposition. We used Image J software (ver. 1.46r) to examine the TEM images.

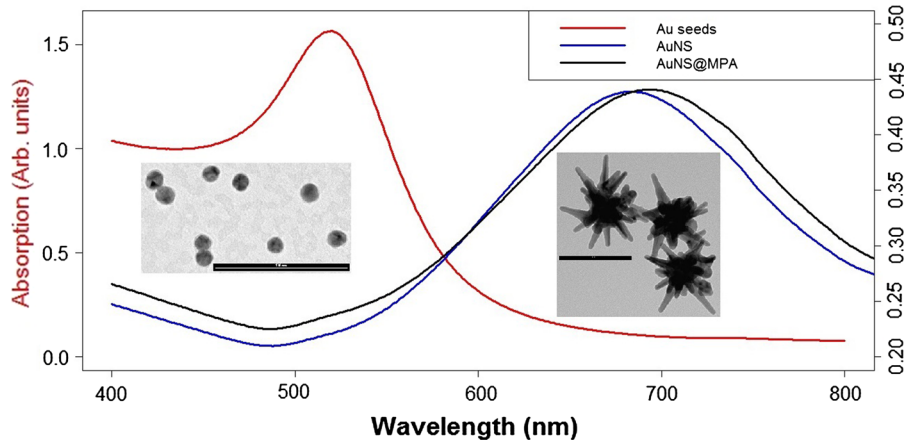

Fig. 1 UV–vis absorption spectra of spherical Au seed (*red*), nanostars (*blue*), and MPA-coated nanostars (*black*). *Insets* TEM images of gold seeds and nanostars. The *scale bars* shown correspond to 100 nm. (Color figure online)

Results and discussion

Figure 1 shows a TEM image of the typical nanostars and one of the gold spherical particles used as seeds, together with their characteristic UV–vis extinction spectra. The gold spheres are highly monodisperse and have a mean diameter of 12.0 ± 0.4 nm. A suspension of such seeds exhibits a spectrum with a sharp absorption maximum at 520 nm. The nanostars, on the other hand, have a broader size distribution with an average diameter of 78 ± 13 nm (measured from tip to tip across the nanostar). TEM images reveal that a single nanostar can contain sharp as well as blunt tips. The UV–Vis spectrum obtained from the nanostars has a broader absorption peak at about 680 nm. We measured the absorption spectrum again after coating the nanostars with MPA. The primary absorption peak red-shifts by 10 nm, which is associated with the formation of a layer of MPA on the surface of the nanostars.

We examined six batches of nanostars for this report. Three were surfactant-free, while the rest were coated with MPA. Figure 2 summarizes the changes in absorption maximum wavelength (λ_{abs}) of different batches of nanostars. For surfactant-free nanostars denoted by SF1, SF2, and SF3, λ_{abs} decreases with time indicating changes in the nanostar tip radius. Centrifugation and filtration do not effectively halt the aging process. λ_{abs} continues to decrease in the following days of observation and the fall-off rate varies for different batches. SF1 has an initial absorbance at 689 nm and has the fastest decay rate, decreasing by as much as 67 nm within 9 days of

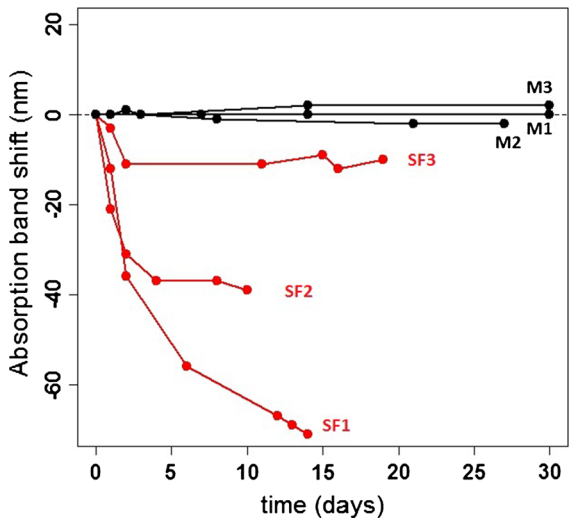

Fig. 2 Shift of the wavelength at maximum absorption upon aging at 4 °C of surfactant-free (SF1, SF2, and SF3) and MPA-capped nanostars (M1, M2, and M3). The confidence on the wavelength is of the order of the dimensions of the data points

aging. SF2 has an initial λ_{abs} at 672 nm and it only decreased by 37 nm in a span of 9 days. The slowest decay rate was observed for SF3 with an initial λ_{abs} at 693 nm and only decreased by 11 nm in 9 days. To show the long-term behavior of surfactant-free nanostars, we measured the UV–vis spectra of SF1 after 11 months. The suspension continues to decay, as evident from the further decrease of λ_{abs} and change in color. SF1 turned to purple with λ_{abs} of 585 nm. As we have noted, the different batches of surfactant-free nanostars have different aging kinetics. We are

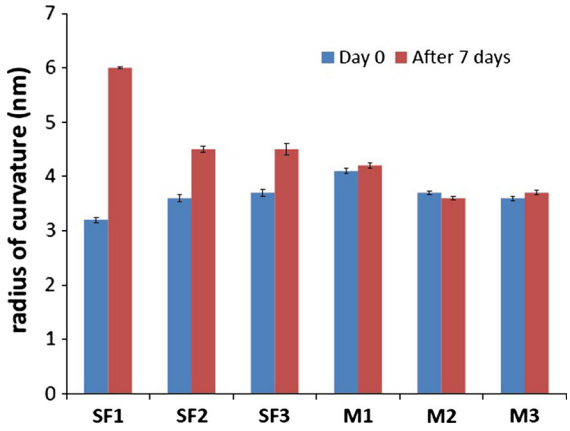

Fig. 3 Changes in the mean radius of curvature (calculated over 200 nanostar tips) of freshly prepared (Day 0) and aged nanostars (after 7 days). *Error bars* represent one standard error

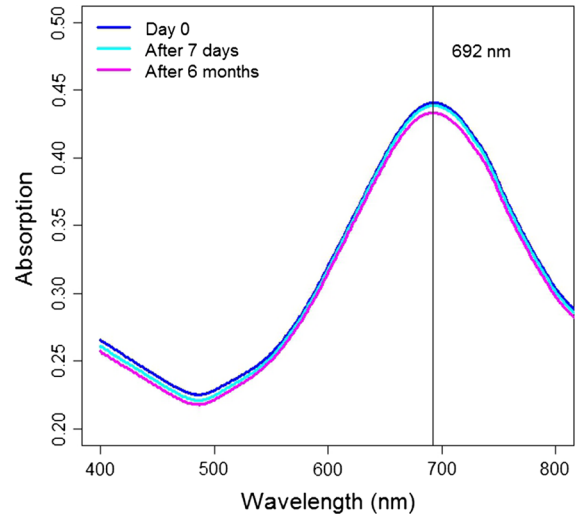

Fig. 4 Extinction spectra of MPA-coated nanostars, M1, recorded on day 0, after 7 days, and after 6 months

currently investigating whether the starting primary absorbance peak can possibly be the determinant of this decay rate. However, from the examples we presented in this paper, no conclusive correlation can be made. More tests should be done on this.

To support our hypothesis that such changes in the extinction spectra can be explained in terms of morphological variations, we measured the radius of curvature of the nanostar tips. In Fig. 3, the radius of curvature of the nanostar tips after aging in solution at 4 °C is reported. Each column represents the average of about 200 tips measured from the TEM images and the bar represents the standard error. For the three batches of surfactant-free nanostars (SF1, SF2, and SF3), we report the average radius of curvature of the tip at day 0 (right after synthesis and filtration) and after one week of aging. For the three batches of MPA-capped nanostars (M1, M2, and M3), we report the radius at day 0 and after 30 days. The radius of the surfactant-free nanostars aged in solution for more than one week is consistently higher than the ones measured on the day of synthesis. On the other hand, no significant change is evident for the MPA nanostars even after 30 days. In Fig. 4, we show the extinction spectra of M1 for day 0, after 7 days, and after 6 months. The fact that the spectra remain unchanged confirms that there are no changes in the nanostar tips radius.

An example of blunting of the tips in surfactant-free nanostars is presented in Fig. 5, which shows the nanostar SF1 at day 0, after 7 days, and after 11 months. At the bottom panel of Fig. 5, it is worth noting that the extinction spectrum after 11 months almost resembles that of a spherical particle with a larger diameter. This means that the contribution of the longitudinal mode to the plasmon resonance has decreased due to the loss of sharp protrusions. This is consistent with the observed decrease in the plasmon resonance wavelength of nanorods, which are comparable to the spikes of the nanostars, with decreasing aspect ratio (Vigderman et al. 2012; Huang et al. 2009). We are led to conclude that the gold atoms from the tips are migrating toward the core and filling the valleys, in a mechanism analogous to a typical sintering process whereby atoms move from convex to concave regions driven by the chemical potential difference associated to the respective curvatures (Kingery et al. 1976). We hypothesize that upon addition of MPA on the surface of the nanostars, the Au–S bond limits the mobility of Au atoms via surface diffusion and kinetically hinders the diffusion of the Au atoms from tips toward the core.

Conclusion

Caution should be exercised when using surfactant-free suspensions of nanostars as they undergo rapid

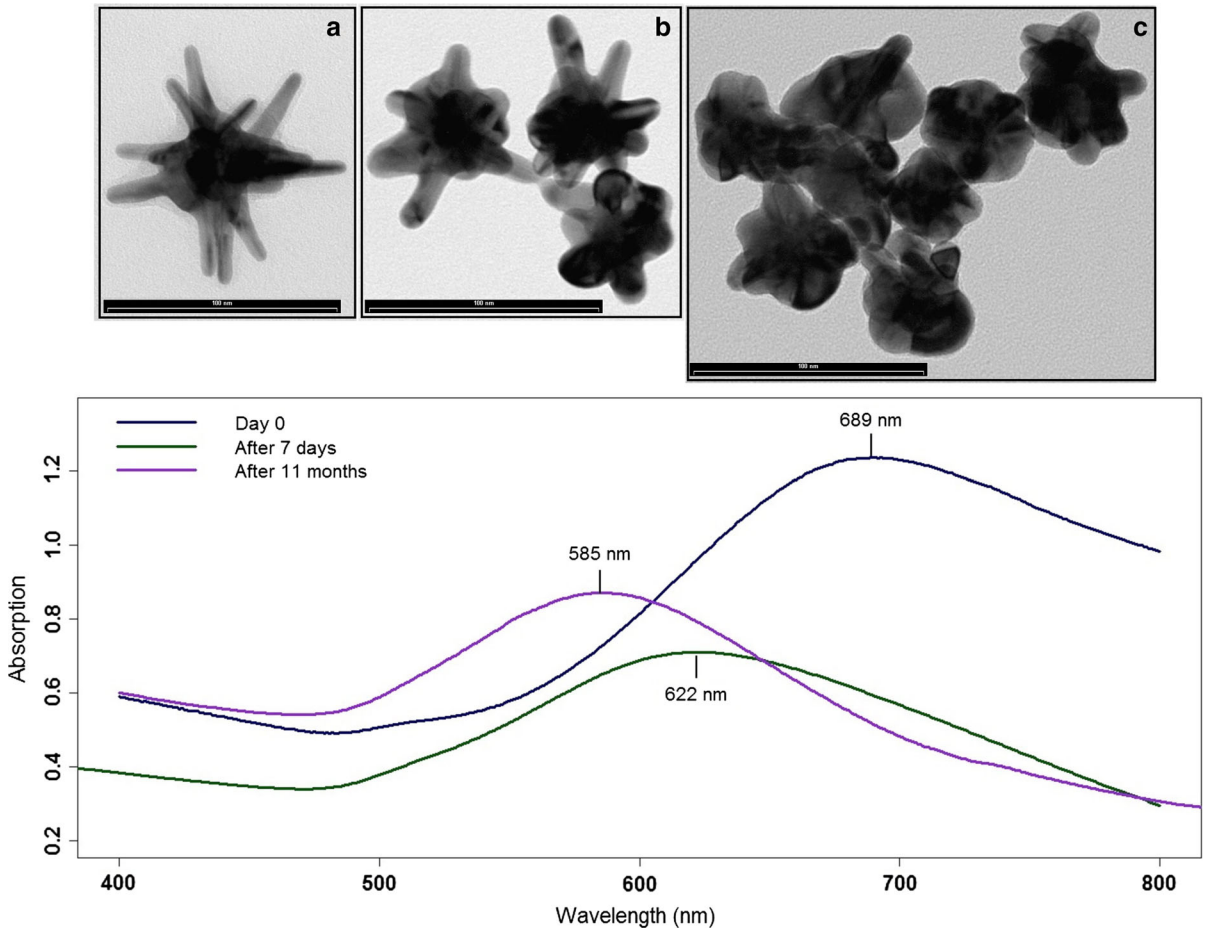

Fig. 5 TEM image of nanostar SF1 at Day 0 (**a**), after 7 days (**b**), and after 11 months (**c**) (the *scale bars* shown represent 100 nm); (*Bottom*) extinction spectra of the same nanostars of **a**, **b**, and **c**

morphological evolution especially during the first few days after synthesis. The rate of decrease in the absorption maximum wavelength, as a consequence of the decrease in the aspect ratio of the nanostar spikes, slows down but does not plateau even after several months of aging. The surfactant-free nanostars, after almost one year of aging in suspension, become more spherical in shape with larger diameter compared to the seeds used in producing them. Aging is the result of migration of atoms from the convex tips to concave valleys toward the core of the nanostars. Such aging can be prevented by capping the nanostar surface with a thiolated compound such as MPA, without greatly affecting the optical property of the nanostars. From our study, we find that MPA-coated nanostars exhibit much longer stability than surfactant-free nanostars.

Acknowledgments Marienette Morales Vega acknowledges the partial support from EU project LONGLIFE. Alois Bonifacio and Valter Sergo acknowledge the financial support from Fondo Ricerca Ateneo (FRA), University of Trieste.

References

Ahmed W, Kooij ES, van Silfhout A, Poelsema B (2010) Controlling the morphology of multi-branched gold nanoparticles. Nanotechnology 21:125,605-1-6. doi:10.1088/0957-4484/21/12/125605

Allijn IE, Leong W, Tang J, Gianella A, Mieszawska AJ, Fay F, Ma G, Russell S, Callo CB, Gordon RE, Korkmaz E, Post JA, Zhao Y, Gerritsen HC, Thran A, Proksa R, Daerr H, Storm G, Fuster V, Fisher EA, Fayad ZA, Mulder WJM, Cormode DP (2013) Gold nanocrystal labeling allows low-density lipoprotein imaging from the subcellular to macroscopic level. ACS Nano 7(11):9761–9770. doi:10.1021/nn403258w

Casu A, Cabrini E, Dona A, Falqui A, Diaz-Fernandez Y, Milanese C, Taglietti A, Pallavicini P (2012) Controlled synthesis of gold nanostars by using a Zwitterionic surfactant. Chemistry 18(30):9381–9390. doi:10.1002/chem.201201024

Cavallaro G, Triolo D, Licciardi M, Giammona G, Chirico G, Sironi L, Dacarro G, Don A, Milanese C, Pallavicini P (2013) Amphiphilic copolymers based on poly[(hydroxyethyl)-d, l-aspartamide]: a suitable functional coating for biocompatible gold nanostars. Biomacromolecules 14(12):4260–4270. doi:10.1021/bm401130z

Cheng Y, Meyers JD, Broome AM, Kenney ME, Basilion JP, Burda C (2011) Deep penetration of a PDT drug into tumors by noncovalent drug-gold nanoparticle conjugates. J Am Chem Soc 133(8):2583–2591. doi:10.1021/ja108846h

Esenturk EN, Walker ARH (2009) Surface-enhanced Raman scattering spectroscopy via gold nanostars. J Raman Spectrosc 40:86–91. doi:10.1002/jrs.2084

Gao J, Huang X, Liu H, Zan F, Ren J (2012) Colloidal stability of gold nanoparticles modified with thiol compounds: bioconjugation and application in cancer cell imaging. Langmuir 28(9):4464–4471. doi:10.1021/la204289k

Guerrero-Martinez A, Barbosa S, Pastoriza-Santos I, Liz-Marzan LM (2011) Nanostars shine bright for you: colloidal synthesis, properties and applications of branched metallic nanoparticles. Curr Opin Colloid Interface Sci 16:118–127

Hao F, Nehl CL, Hafner JH, Nordlander P (2007) Plasmon resonances of a gold nanostar. Nano Lett 7(3):729–732. doi:10.1021/nl062969c

Hrelescu C, Sau TK, Rogach AL, Jackel F, Feldmann J (2009) Single gold nanostars enhance Raman scattering. Appl Phys Lett 94:153,113-1-3. doi:10.1063/1.3119642

Huang X, Neretina S, El-Sayed MA (2009) Gold nanorods: from synthesis and properties to biological and biomedical applications. Adv Mater 21(48):4880–4910. doi:10.1002/adma.200802789

Jarvis RM, Goodacre R (2004) Discrimination of bacteria using surface-enhanced Raman spectroscopy. Anal Chem 76(1):40–47. doi:10.1021/ac034689c

Jeong GH, Lee YW, Kim M, Han SW (2009) High-yield synthesis of multi-branched gold nanoparticles and their surface-enhanced Raman scattering properties. J Colloids 329(1):97–102. doi:10.1016/j.jcis.2008.10.004

Kastanos EK, Kyriakides A, Hadjigeorgiou K, Pitris C (2009) A novel method for urinary tract infection diagnosis and antibiogram using Raman spectroscopy. J Raman Spectrosc 41:958–963. doi:10.1002/jrs.2540

Khoury CG, Vo-Dinh T (2008) Gold nanostars for surface-enhanced raman scattering: synthesis, characterization and optimization. J Phys Chem C 112(48):18,849–18859. doi:10.1021/jp8054747

Kingery WD, Uhlmann DRDR, Bowen HK (1976) Introduction to ceramics, 2nd edn. Wiley, New York

Kooij E, Ahmed W, Hellenthal C, Zandvliet H, Poelsema B (2012) From nanorods to nanostars: tuning the optical properties of gold nanoparticles. Colloids Surf A 413:231–238. doi:10.1016/j.colsurfa.2012.01.041

Kumar PS, Pastoriza-Santos I, Rodriguez-Gonzalez B, de Abajo FJG, Liz-Marzan LM (2008) High-yield synthesis and optical response of gold nanostars. Nanotechnology 19:015,606-1-6. doi:10.1088/0957-4484/19/01/015606

Liu Y, Wu P (2013) Meditating metal coenhanced fluorescence and sers around gold nanoaggregates in nanosphere as bifunctional biosensor for multiple dna targets. ACS Appl Mater Interfaces 5(12):5832–5844. doi:10.1021/am401468a

Nam J, La WG, Hwang S, Ha YS, Park N, Won N, Jung S, Bhang SH, Ma YJ, Cho YM, Jin M, Han J, Shin JY, Wang EK, Kim SG, Cho SH, Yoo J, Kim BS, Kim S (2013) pH responsive assembly of gold nanoparticles and spatiotemporally concerted drug release for synergistic cancer therapy. ACS Nano 7(4):3388–3402. doi:10.1021/nn400223a

Pallavicini P, Dona A, Casu A, Chirico G, Collini M, Dacarro G, Falqui A, Milanese C, Sironi L, Taglietti A (2013) Triton X-100 for three-plasmon gold nanostars with two photothermally active NIR (near IR) and SWIR (short-wavelength IR) channels. Chem Commun 49:6265–6267. doi:10.1039/C3CC42999G

Rodriguez-Lorenzo L, Romo-Herrera JM, Perez-Juste J, Alvarez-Puebla RA, Liz-Marzan LM (2011) Reshaping and LSPR tuning of Au nanostars in the presence of CTAB. J Mater Chem 21:11,544–11549

Rodriguez-Oliveros R, Sanchez-Gil JA (2012) Gold nanostars as thermoplasmonic nanoparticles for optical heating. Opt Express 20(1):621–626

Sironi L, Freddi S, Caccia M, Pozzi P, Rossetti L, Pallavicini P, Don A, Cabrini E, Gualtieri M, Rivolta I, Panariti A, DAlfonso L, Collini M, Chirico G (2012) Gold branched nanoparticles for cellular treatments. J Phys Chem C 116(34):18,407–18,418. doi:10.1021/jp305021k

Tamburro D, Fredolini C, Espina V, Douglas TA, Ranganathan A, Ilag L, Zhou W, Russo P, Espina BH, Muto G, Petricoin EF, Liotta LA, Luchini A (2011) Multifunctional core-shell nanoparticles: discovery of previously invisible biomarkers. J Am Chem Soc 133(47):19,178–19188. doi:10.1021/ja207515j

Trigari S, Rindi A, Margheri G, Sottini S, Dellepiane G, Giorgetti E (2011) Synthesis and modeling of gold nanostars with tunable morphology and extinction spectrum. J Mater Chem 21:6531–6540. doi:10.1039/c0jm04519e

Vigderman L, Khanal BP, Zubarev ER (2012) Functional gold nanorods: synthesis, self-assembly, and sensing applications. Adv Mater 24(36):4811–4841. doi:10.1002/adma.201201690

Wheeler DA, Green TD, Wang H, Fernandez-Lopez C, Liz-Marzan L, Zou S, Knappenberger KL, Zhang JZ (2012) Optical properties and coherent vibrational oscillations of gold nanostars. Chem Phys Lett 543:127–132. doi:10.1016/j.cplett.2012.06.058

Wu HL, Chen CH, Huang MH (2009) Seed-mediated synthesis of branched gold nanocrystals derived from the side growth of pentagonal bipyramids and the formation of gold nanostars. Chem Mater 21:110–114

Yuan H, Fales AM, Khoury CG, Liu J, Vo-Dinh T (2012a) Spectral characterization and intracellular detection of surface-enhanced Raman scattering (SERS)-encoded plasmonic gold nanostars. J Raman Spectrosc 44:234–239

Yuan H, Fales AM, Vo-Dinh T (2012b) TAT peptide-functionalized gold nanostars: enhanced intracellular delivery and efficient nir photothermal therapy using ultralow irradiance. J Am Chem Soc 134(28):11,358–11361. doi:10.1021/ja304180y

Yuan H, Khoury CG, Hwang H, Wilson CM, Grant GA, Vo-Dinh T (2012c) Gold nanostars: surfactant-free synthesis, 3D modelling, and two-photon photoluminescence imaging. Nanotechnology 23(7):075,102